Heat and Mass Transfer 40 (2004) 679–688
DOI 10.1007/s00231-003-0433-0

Thermal contact conductance for cylindrical and spherical contacts

S. Sunil Kumar, P. M. Abilash, K. Ramamurthi

Abstract A prediction methodology based on Monte-Carlo simulation model, developed for flat conforming surfaces in contact, is modified and extended to predict contact conductance between curvilinear surfaces like cylinders and spheres. Experiments are also conducted in vacuum for the measurement of contact conductance between stainless steel and aluminium cylindrical contacts and stainless steel spherical contacts over a range of contact pressures. The contact conductance between cylindrical and spherical bodies is, in general, about an order of magnitude lower than for flat surfaces in contact. Increase of surface roughness and decrease in contact pressure lowers the contact conductance. However, the influence of these parameters is larger than those obtained for flat surfaces. The prediction for different parametric conditions agree closely with those measured in the experiments.

List of Symbols

a, b	semi-axes of the elliptical contact zone, m
A	area, m^2
d	diameter of the sample, m
E	Young's modulus, Pa
h_t	thermal contact conductance, W/m^2 K
H	micro hardness of the softer material, Pa
h^*	dimensionless contact conductance defined by Eq. (31)
k	harmonic mean of thermal conductivities, W/m K
m	slope of the asperity
N_j	Number of asperities in a discretised region, j
N_T	density of asperities, per m^2
n_c	number of contacting asperities
P	contact pressure, Pa
P^*	dimensionless pressure defined by Eq. (31)
Q	heat flow rate, W
r	contact spot radius of asperities, m
R	radius of curvature of the contact surface, m
R_a	mean surface roughness, m
R_s, R_c, R_t	resistance due to roughness, area contour and total respectively
ΔT	temperature difference
U_x	Gaussian random number
x	summit heights, m
δ	summit penetration depth, m
ε	clearance between the surfaces, m
σ	standard deviation in summit heights, m
ψ	constriction alleviation factor

Subscripts

a	apparent
c	contact/contour
i	i^{th} asperity
j	j^{th} discretised region
1, 2	surfaces 1 and 2

Received: 22 July 2002
Published online: 13 May 2003

S. Sunil Kumar, P. M. Abilash, K. Ramamurthi (✉)
Propulsion Research and Studies Group,
Liquid Propulsion Systems Centre,
Trivandrum, Kerala, India, 695 547
E-mail: ram123@md2.vsnl.net.in

1 Introduction

A large number of experimental and theoretical studies [1–5] has been reported on thermal contact conductance across joints. Most of them relate to flat surface contacts. Very few of these studies consider joints formed between cylinders and flat surfaces, between spheres or between spheres and cylinders. The role of curvature at the contact has not been adequately understood even though such contacts are important in several applications such as plug and ring assemblies, shrink-fit cylinders, finned tube heat exchangers, nuclear reactor fuel elements and bearings. The present investigation deals with contact conductance of joints involving cylindrical and spherical surfaces.

A detailed review of thermal contact conductance of cylindrical joints was presented by Madhusudhana et al. [6]. The study dealt with circumferential cylindrical contacts such as encountered in shrink-fit cylinders. Sheffield et al. [7] dealt with mechanically expanded copper tubes with aluminium fins. Dart [8] and Gardner and Carnavos [9] pioneered the investigation in the area of interference fitted tubes. Gardner and Carnavos noted that as the temperature increased, the fins expanded away from the tube walls and greater proportion of the heat was transferred through the gas gaps at the interface than through actual metal to metal contact spots. A situation was eventually reached where the gap between the fin base and the tube was opened to such an extent that no heat was transferred through the solid spots. These early observa-

tions were supported by the calculations of Kulkarni and Young [10].

Spheres in elastic contact with bare flat surfaces were investigated by Kitscha and Yovanovich [11]. They experimentally verified the analytical solution in the elastic load range. Fischer and Yovanovich [12] investigated both theoretically and experimentally the thermo mechanical problem of a stainless steel sphere in elastic contact with a nickel flat coated with silver layer. A simple analytical model developed using Hertzian limits for the mechanical aspects of contact showed reasonable results with the experiments.

Heat conduction between rolling contacts at different temperatures was addressed by Bejan [13]. Here the contact region is modeled according to the classical Hertz theory. The results show that when two bodies make contact continuously over an elliptical area, the overall heat transfer rate is proportional to the square root of the Peclet number based on the ellipse semi-axis and also on the square root of the normal force between the two bodies.

Greenwood and Tripp [14] analysed the problem of thermal contact conductance between rough spheres in elastic contact. They showed that the presence of discrete contact sites (asperities) does not affect the size and shape of the macroscopic elliptical contact region at sufficiently high loads. Schneider et al. [15] analysed the transient thermal response of two bodies communicating through a small circular contact area.

Yovanovich and Kitscha [16] modeled the effect of air and oil upon the thermal resistance of a sphere – flat contact as a function of solid constriction resistance. The elastic theory was used and radiative heat transfer and conduction resistance of the gas gap as a function of gas pressure ranging from vacuum to atmospheric conditions were considered. The predictions were compared with the test data and found to be in good agreement.

The above studies carried out in the area of cylindrical and spherical contacts, do not address a generalised model for 'apriori' predictions of the contact conductance at the curved surfaces for different surface characteristics, loading conditions and materials. The present work is in this direction and focuses on the development of a model to predict thermal conductance at contacts formed between curved surfaces.

2
Theoretical formulation

Heat flowing between two bodies in ideal contact with each other must flow through the solid contact area. The constriction of the heat flow lines at the contacting surfaces gives rise to the thermal resistance which is defined as the temperature difference across the contact divided by the total heat flow rate through the contact. This resistance depends upon the load, geometry and thermophysical properties of the contact. The theoretical formulation for the estimation of thermal contact conductance between geometries therefore primarily models the contacting surfaces.

3
Contact region between curved surfaces

(a) Contour area of contact The resistance to flow of heat in a contact zone is due to the reduced area of contact actually available compared to the apparent area of contact. In the case of contacting surfaces which are cylindrical or spherical, heat is first constrained to flow through the contour area of contact formed due to curved surfaces in contact and is then constrained to flow through the microscopic contact region formed due to surface roughness. According to Hertz classical theory [17], the contour of the contact area has the shape of an ellipse. The pressure distribution is represented by a semi-ellipsoid constructed on the contact area when two spherical or cylindrical bodies are pressed in elastic contact. This is sketched in Fig. 1, where the contact surface lies in the plane x–y as shown. The linear dimensions a and b of this contact region (Fig. 1) is considerably smaller than the smallest of the principal radii of curvature of the two body surfaces that come into contact. The contact surface can be taken to be planar regardless of the relative elasticity of the two bodies [17]. Timoshenko and Goodier [18], arrive at the values a and b of the semi-axes of the contact area as:

$$a = M\left[\frac{3\pi(k_1 + k_2)}{4(A + B)}F\right]^{1/3} \tag{1}$$

$$b = N\left[\frac{3\pi(k_1 + k_2)}{4(A + B)}F\right]^{1/3} \tag{2}$$

Here, F is the total force with which one body pushes against the other,

$$k_1 = \frac{1 - R_1^2}{\pi E_1}, \quad k_2 = \frac{1 - R_2^2}{\pi E_2} \tag{3}$$

and A and B are geometrical parameters and given by:

$$2(A + B) = \frac{1}{R_1} + \frac{1}{R_1'} + \frac{1}{R_2} + \frac{1}{R_2'} \tag{4}$$

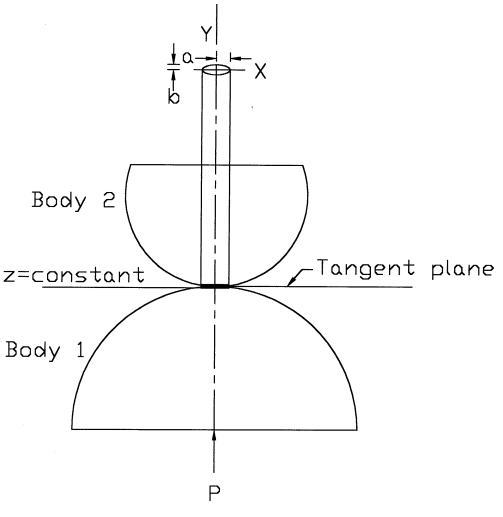

Fig. 1. Profiles of contacting surfaces

(R_1, R'_1) and (R_2, R'_2) are the principal radii of curvature of the two body surfaces in the vicinity of contact.

The coefficients M and N in Eqs. (1) and (2) are geometric parameters as they depend only on the dimensionless group (B – A)/(A + B). This dependence is tabulated for small values of this group in Timoshenko and Goodier [18] and for large values in Kornhauser [19]. Bejan [13] combined these two results in a tabular form. Knowing the semi-axes a and b, the pressure distribution over the elliptical contact area is obtained to be [13]:

$$P(x, y) = P_0\left[1 - \left(\frac{x}{a}\right)^2 - \left(\frac{y}{b}\right)^2\right]^{1/2} \tag{5}$$

where P_0 is the maximum contact pressure. This maximum pressure is located at the centre of the contact spot and is given by:

$$P_0 = \frac{3}{2}\left(\frac{F}{\pi ab}\right) \tag{6}$$

(b) Reduced area of contact Any machined surface will have a certain degree of surface roughness quantified by a roughness parameter R_a which is the average height of the profile above and below a mean line. When two surfaces are in contact, surface roughness leads to individual microscopic contacts due to interaction of asperities from the two surfaces. Assuming that the most probable distribution of asperity heights is Gaussian, the distribution of asperity heights for a surface is described by a standard deviation of combined height distribution (σ) and an average slope (m) for the asperities and is given by Leung et al. [4] as:

$$f(x) = \frac{1}{\sqrt{2\pi}\sigma}\exp\left[-\frac{1}{2}\left\{\frac{x - R_a}{\sigma}\right\}^2\right] \tag{7}$$

The density of surface asperity is also given as

$$N_T = (m/7.308\,\sigma)^2 \tag{8}$$

with the maximum summit height as

$$x_{max} = 8\,\sigma \tag{9}$$

The mean summit height which is same as the average height of protrusions on the surface is given by:

$$R_a = 4\,\sigma \tag{10}$$

The asperity density and the maximum and mean summit height are used to model the true contact area. When opposing asperities of height x_1 and x_2 come into contact with each other, the asperity height undergoes a plastic deformation. Based on simple geometry (shown in Fig. 2), this results in the contact spot radii, r

$$r = 0 \quad \text{if } \delta \le 0 \tag{11}$$

$$r = \delta/2\,m \quad \text{if } \delta > 0 \tag{12}$$

Here δ is the summit penetration depth depicted in Fig. 2. A value of δ less than zero implies that the two asperities

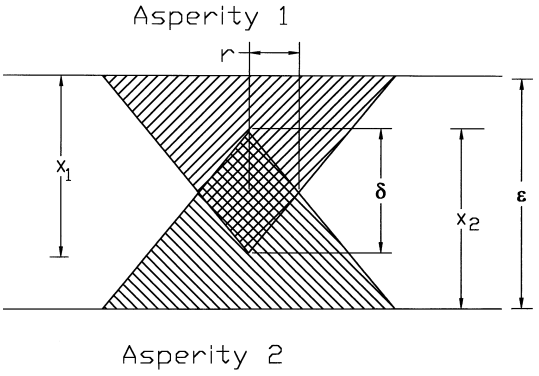

Fig. 2. Idealised contact element

are not in contact. The separation distance between the reference planes of the two contacting surfaces, otherwise defined as the average clearance between the surfaces, is given by:

$$\varepsilon = \sqrt{2}\sigma\ \mathrm{erfc}^{-1}\left(\frac{2P}{P + H}\right) \tag{13}$$

The above expression for clearance takes into account the material hardness, the surface roughness and the contact pressure. The reduced area of contact is determined from the contact spot radii. For conforming flat surfaces, the pressure term in Eq. (13) corresponds to overall contact pressure based on the apparent area of contact. However, for non-flat surfaces, the pressure would vary in different contact zones of the contour region. The contour region is therefore subdivided into large number of elemental areas within which the pressure is assumed to be the same. This is dealt with subsequently.

4
Heat transfer through the reduced area of contact

The heat flow under steady state conditions across the joint will be constrained at macro level through the contour zones corresponding to macro constrictions from curved surfaces and then further constrained through the individual micro contacts. In addition to the micro surface constriction resistance (R_s), there is an additional macroscopic contact resistance (R_c) [20, 21] due to area contours formed by curvature. The total constriction resistance R_t is therefore given by:

$$R_t = R_s + R_c \tag{14}$$

The total contact conductance, h_t is determined as:

$$h_t = \frac{1}{R_t A_a} \tag{15}$$

The resistance due to roughness (R_s) is distributed among the contact spots of different sizes existing at the contact plane. Once the individual contact spot radii, r_i are known, the heat flow rate for each individual contact spot can be written as:

$$Q_i = 2k\,r_i\,\Delta T_c(1/\psi_i) \tag{16}$$

where ΔT_c is the temperature drop across the interface.

ψ_i in Eq. (16) is a geometrical factor equal to unity for a single contact belonging to an infinite apparent area. For appropriately distributed contacts having contact points at the centre of the corresponding asperities, a simple expression that closely approximates the analytical and numerical solution is given by Madhusudana [22] to be:

$$\psi_i = \left[1 - \left(\frac{P}{H}\right)^{1/2}\right]^{1.5} \tag{17}$$

Variation in ψ is neglected from contact to contact in the present analysis and is considered to be the same following Madhusudana [22]. If there are n_c contacting asperities over an apparent area A_a, the total heat flow across the joint is given by:

$$Q = \sum_{i=1}^{n_c} Q_i \cong \frac{2k\Delta T_c}{\psi} \sum_{i=1}^{n_c} r_i \tag{18}$$

The thermal resistance due to surface roughness alone can be determined from the preceding equation to be

$$R_s = \frac{\Delta T_c}{Q} = \frac{\psi}{2k \sum_{n_c} r_i} \tag{19}$$

Here n_c represents the number of contacting asperities; r_i is the radius of each individual contact circle formed by two contacting asperities (see Fig. 2) and k is the harmonic mean of the conductivities of the two contacting materials. The value of Σr_i is obtained from of the geometry of the contacting surfaces and surface parameters and is detailed in the following sections.

The macro resistance of area contours formed by the curved surfaces (R_c) is written following [22] as:

$$R_c = \frac{\psi_c}{2ka_c} \tag{20}$$

The macro surface constriction parameter ψ_c in the above equation is estimated using the expression developed by Roess [23] which gives,

$$\psi_c = 1 - 1.4093(x_c) + 0.2959(x_c)^3 + 0.0525(x_c)^5 \tag{21}$$

where

$$x_c = \frac{a_c}{r_a} \tag{22}$$

Here, a_c represents the equivalent radius of the contour area formed by the contacting curvilinear surfaces and r_a is the radius of the apparent area of contact. The total contact conductance can be written from Eq. (15) as:

$$h_t = \frac{1}{\left[\frac{\psi}{2k \sum_{n_c} r_i} + \frac{\psi_c}{2ka_c}\right] A_a} \tag{23}$$

(a) Estimation of radius of individual contact spots It is essential to determine the number of contacting asperities and their radius of contact r_i for estimating the thermal contact conductance given by Eq. (23). In the present study the geometries considered are curvilinear and the contour area of contact can be estimated as given earlier using Hertz classical theory. However, unlike the uniform distribution of contacting asperities in the case of conforming flat surfaces, the contacting asperities are non-uniform due to the curvature of the contacting surfaces. The higher nominal pressure near the centre of the ellipse of contact (Fig. 1) is modeled in the present analysis as equivalent to the formation of denser population of contact site leading to a non-uniform distribution of contact sites. The model is illustrated in Fig. 3 by variation in the density of the contacting asperities. The changes in number of contact points in each layer is decided by the curvature of the contacting surfaces. At the centre of the ellipse the clearance between the two contacting surfaces is given by ε defined by Eq. (13). Away from the centre there is an additional clearance introduced due to the curvature of the contacting surface. To accommodate these density changes the contact elliptical zone is discretised into numerous small ellipsoids as shown in Fig. 4.

The number of asperities in a discretised contact zone of area A_j is given by,

$$N_j = N_T \times A_j \tag{24}$$

If x_{max1} and x_{max2} are the respective maximum asperity heights due to roughness of Surface 1 and Surface 2 respectively and if we choose randomly one asperity each on either surface of height x_1 and x_2, then

$$x_1/x_{max\,1} \leq 1 \quad \text{and} \quad x_2/x_{max\,2} \leq 1 \tag{25}$$

The ratio of x_1/x_{max1} and x_2/x_{max2} could take any Gaussian random number U_x between 0 and 1, that is;

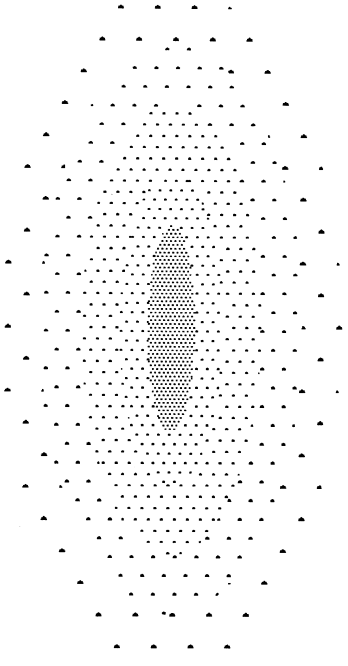

Fig. 3. Hertzian elliptical contact area

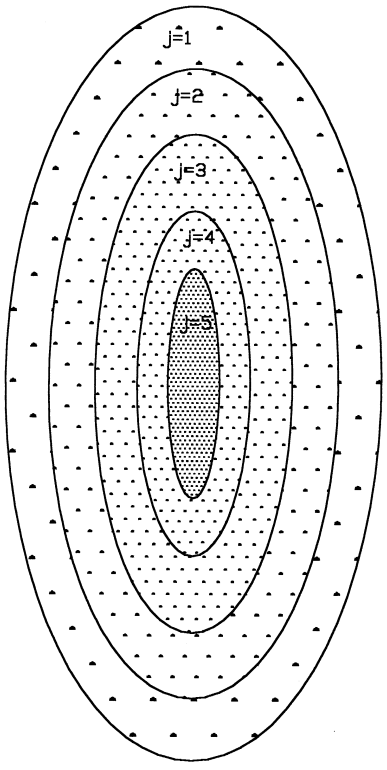

Fig. 4. Discretisation of contact site into regions of uniform distribution of contacting asperities

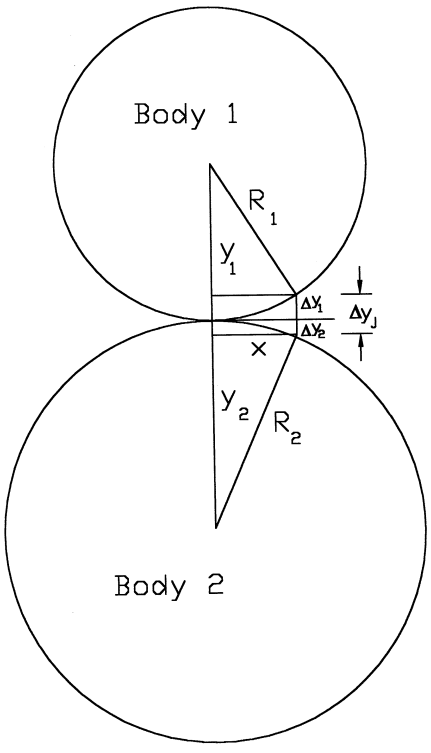

Fig. 5. Physical representation of contact geometry

$$x_1/x_{max\,1} = U_{x1} \quad \text{and} \quad x_2/x_{max\,2} = U_{x2} \tag{26}$$

By randomly assigning two Gaussian random numbers U_{x1} and U_{x2}, the individual asperity height of the conforming surfaces can be estimated for the descretised region j. The additional clearance due to curvature effects can be determined by considering two circular sections each of radius R_1 and R_2 in contact at each other as shown in Fig. 5. At a discretised zone j, distance x away from the centre, the additional clearance is represented by Δy_j. From Fig. 5, Δy_j can be determined as

$$R_1 - \Delta y_1 = \sqrt{R_1^2 - x^2} \quad \text{and} \quad R_2 - \Delta y_2 = \sqrt{R_2^2 - x^2} \tag{27}$$

i.e.

$$\Delta y_1 = R_1 - \sqrt{R_1^2 - x^2} \quad \text{and} \quad \Delta y_2 = R_2 - \sqrt{R_2^2 - x^2} \tag{28}$$

The combined additional clearance due to the curvature of both surfaces is therefore given by:

$$\Delta y_j = \Delta y_1 + \Delta y_2 \tag{29}$$

For all the asperities in a descretised zone, at a distance x from the centre, this value is assumed constant and the clearance for a zone is given by $\varepsilon_j = \varepsilon + \Delta y_j$.

If the combined heights of asperities are larger than the total clearance thus estimated for the region, then these asperities will touch each other. The penetration depth of the asperity is given by:

$$\delta = x_1 + x_2 - \varepsilon_j \tag{30}$$

Once δ is known, the spot contact radii, r_i can be calculated from Eq. (12). The analysis is repeated for all the asperities in the contact region. The total number of contact spots (n_c) and their respective contact radii r_i are then determined. By substituting these parameters in Eq. (23), the contact conductance, h_t at the joint is determined.

5
Theoretical predictions

Figure 6 gives a flow chart of the computations. The Gaussian random number, used in the analysis, was generated using the Microsoft Fortran uniform random number generator subroutine RANDOM. The subroutine returns a value between 0 and 1 for an input seed value. For the same input seed value, repeated computations reproduced the predicted values of contact conductance within 0.47%. This variation is slightly higher when compared to that obtained [5] in the case of flat surface contact (0.1%) and is due to the lower number of contact spots available in the small contact region in the present geometry. When the number of random numbers used for the generation of Gaussian random number was doubled, the deviations were found to decrease. The relative difference in the estimated values of conductance for double precision and single precision calculation was less than 0.21% which is again slightly higher compared to those reported [5] for flat surfaces (0.16%).

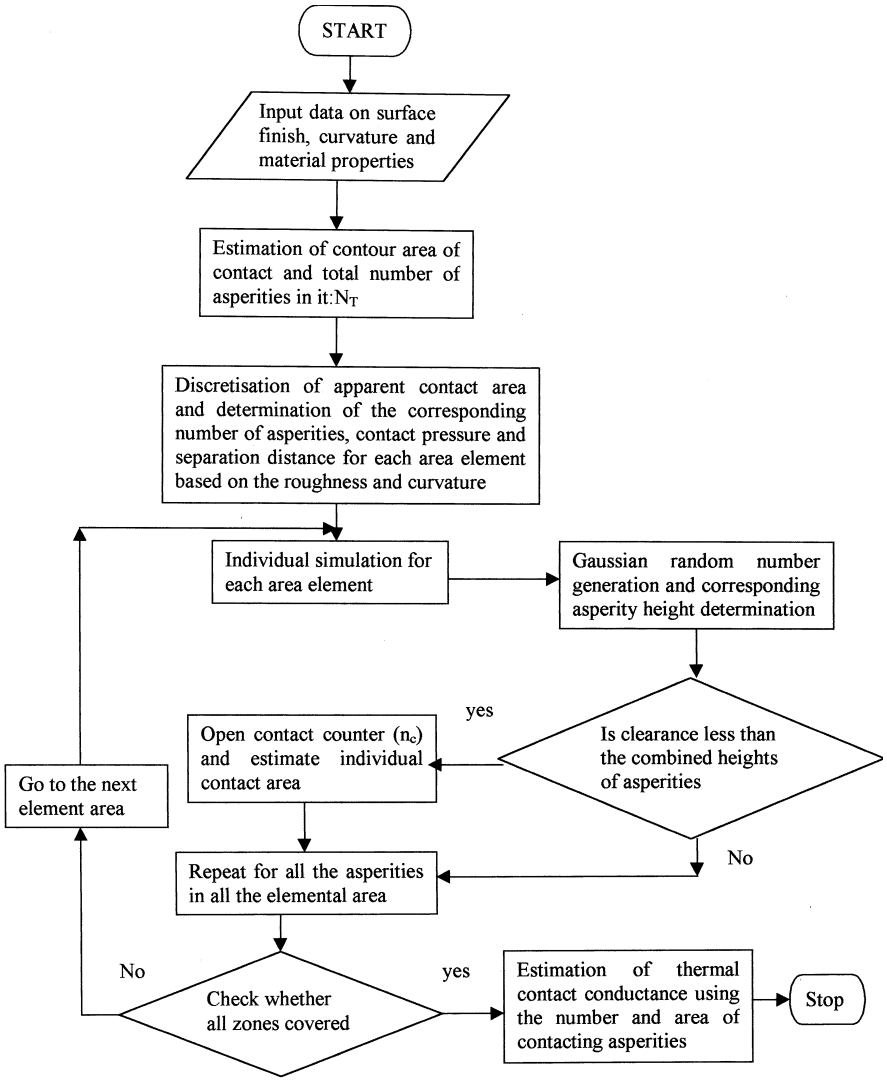

Fig. 6. Computational flow diagram

The model was first validated for the limiting case of conforming flat surface contact, where R_1 and R_2 tend to infinity. Predictions were done for varying surface roughness and contact pressures for different materials. The results were compared with those obtained for flat surface joints given by Leung et al. [4]. The comparison is given in Fig. 7 as dimensionless contact conductance h^* and pressure P^*, defined as:

$$h^* = \frac{h\sigma m}{k} \quad \text{and} \quad P^* = \frac{P}{H} \tag{31}$$

Reasonably good agreement is seen to be obtained over a wide range of contact pressures validating the model.

A large number of computations were carried out by varying the values of parameters such as surface roughness, interfacial contact pressures and materials of contacting surfaces. The analysis is carried out for curved geometrical contacts involving cylinders, spheres and flat surfaces.

6
Variation of contact conductance for different surface geometries

Figure 8 shows the variation in thermal contact conductance for a cylinder to flat surface contact, cylinder to cylinder contact, cylinder to sphere contact and a sphere to sphere contact with changes in contact pressure between 10 MPa and 100 MPa. The material considered is stainless steel with a mean surface roughness of 1.5 μ. Diameter of all the curved surfaces were kept at 30 mm. The values of contact conductance for flat surfaces for the same surface roughness is also included in the figure. It can be seen that cylinder to flat surface contact gives by far the highest thermal contact conductance among the curvilinear joints while the sphere to sphere contact results in the lowest value of thermal contact conductance. The values obtained for flat surfaces in contact are higher by almost an order of magnitude. When curved surfaces are in contact, the heat flow, constrained to flow along the line or point contact region, is further constrained to flow through individual contacting asperities. The variation in their respective contact conductances is a result of the changes in number of contacting asperities in the contact zone. Higher thermal contact conductance represents contact zones with more uniformly distributed denser contacts (Fig. 4).

The rate of change of contact conductance with load is seen form Fig. 8 to be smallest for the sphere to sphere joint. The contact zone in a cylinder to cylinder contact is not represented by an ellipse but by a narrow rectangular

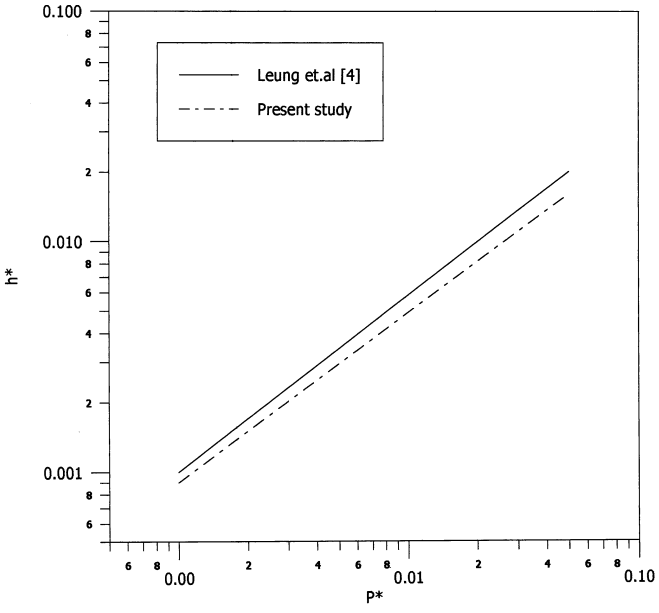

Fig. 7. Comparison with earlier study of Leung et al. [4] for flat contact

strip whose width is given by the minor axis of the Hertzian ellipse. The length of the strip is the length of the cylindrical contact region.

The influence of material hardness is shown in Fig. 9 where predictions are done for stainless steel and aluminium cylinders in contact. Aluminium being a lighter material flows more spontaneously under pressure and thereby increases the contact area leading to higher values of conductance at joints. It may also be noted that the initial response to load for the case of an aluminium joint is more impressive compared to the stainless steel joint.

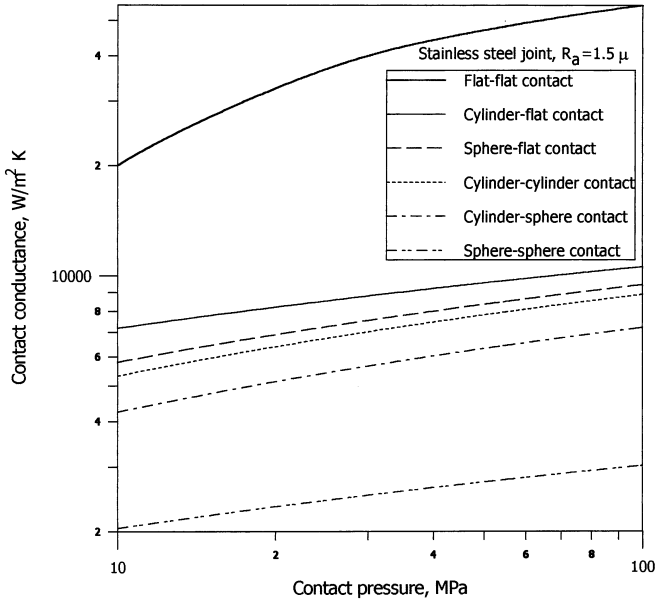

Fig. 8. Variation of thermal contact conductance for different curvilinear contact geometries (Diameter of cylindrical and spherical bodies = 30 mm, Height of the cylinder = 30 mm)

Another important parameter which controls the contact conductance is the surface roughness. The studies done earlier for the case of conforming flat surfaces [5] suggested fine machining to increase the conductance at a joint. Similar trends were obtained in the case of cylindrical contacts and are shown in Fig. 10 for changes in contact conductance values with changes in surface roughness for both aluminium and stainless steel cylindrical contacts. An appreciable difference from flat conforming contact is the more rapid change in conductance for higher values of surface roughness. Since the area of contact at the joint itself is very small, changes in surface asperity heights have a stronger influence on the resultant thermal contact conductance at the joint.

When cylinders are in external contact, the contact conductance is much reduced due to the smaller contact area. The predictions for the external and internal concentric cylindrical contacts are illustrated in Fig. 11. It can be seen that even at no load conditions, the thermal contact conductance for cylinders in contact concentrically shows higher values compared to those for external cylindrical contacts. The differences are larger at higher contact pressures. Higher contact conductance is to be expected for concentric cylindrical contacts due to higher number of contacting asperities.

7 Experiments

Measurements were carried out in vacuum for two typical contact geometries of cylindrical and spherical contacts over a range of contact pressures. The set up used for the experiments were similar to that developed by Sunil Kumar and Ramamurthi [24] for the case of experimental evaluation of thermal contact conductance for flat surfaces with metallic and non-metallic coatings.

Two pairs of stainless steel and aluminium cylindrical rods of 30 mm length and 30 mm width and a pair of

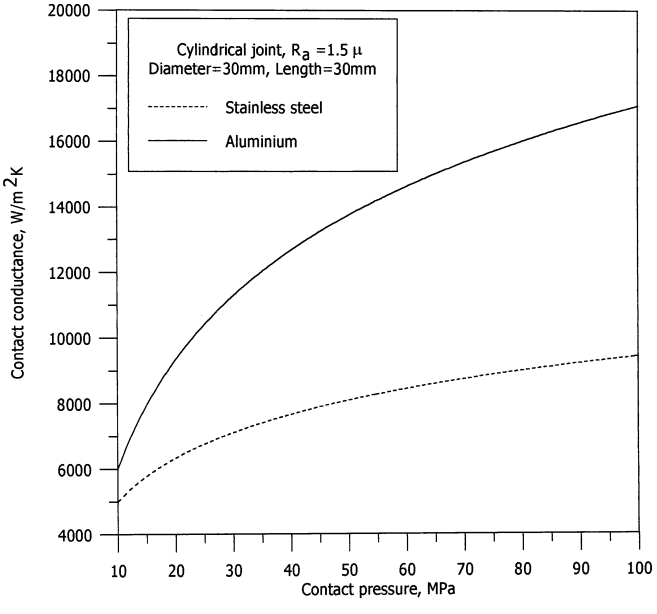

Fig. 9. Effect of material hardness on thermal contact conductance

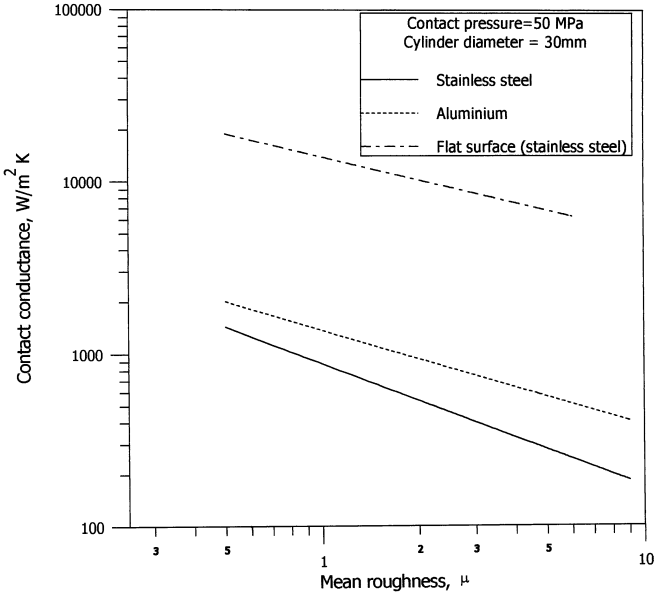

Fig. 10. Variation of thermal contact conductance with surface roughness

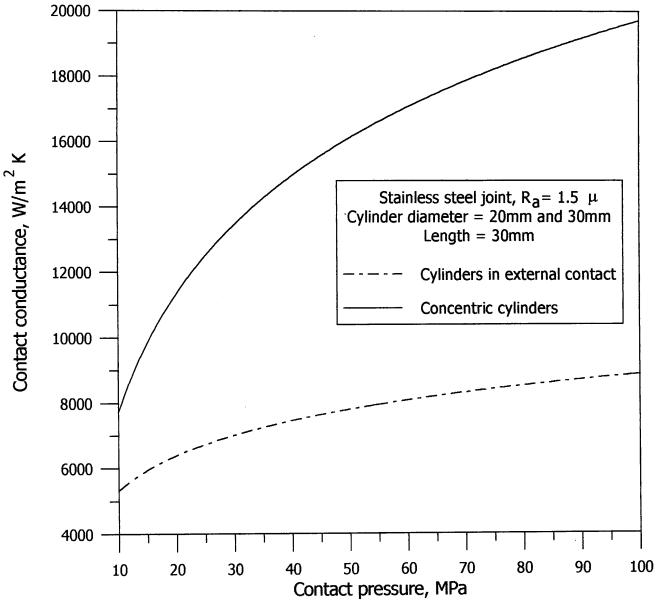

Fig. 11. Comparison of thermal contact conductance for cylinders in external and internal contact

stainless steel sphere of 35 mm diameter are made. In either case, a small portion of cylindrical/spherical surface is machined off to enable proper loading during experiments and is shown in Fig. 12. The test pieces are tightly placed inside the Teflon bracket as shown. The surface finish over the contact region and the out of roundness are evaluated from two-dimensional measurements of surface topography using a Talysurf with a digital read out facility. The surface finish was maintained in between 2 μ to 2.5 μ in the case of cylindrical rods and 1.0 μ in the case of spheres. The out of roundness was well within 0.3 μ for all the surfaces. The measurement accuracy of the Talysurf was ±2% over a range of 0–20 μ.

The surface contact conductance was measured in an axial heat flow apparatus. A sketch of the test apparatus is shown in Fig. 13. The test pieces were heated by a small thermofoil heater of the same size of that of the slotted area of the specimen. The power input to the heater was controlled by a variac and measured through a precision digital wattmeter. The loading of the interface was done by tightening the loading bolt. The resultant load was measured using a load cell placed between the heater and the loading bolt. The contact pressure was varied between 5MPa and 80MPa. An insulator made of Vespel was used to minimize the amount of heat transferred up through the loading bolt. Eight thermocouple junctions of T type were attached to the flat surface of the test specimen 5 mm apart. The thermocouples were welded to the specimen using a discharge type thermocouple-welding machine. The load cell and the thermocouple outputs were connected to a Fluke Hydra series digital multimeter (DMM) with scanner. The test specimens were held together on the side by a C shaped bracket made of Teflon as shown in Fig. 12 so that they do not slip under load.

The setup was placed inside the vacuum chamber of approximately 180-litre capacity. Vacuum was achieved using a two-stage rotary vane vacuum pump and the level of vacuum was measured using a Pirani gauge with digital read out facility. All experiments were conducted at vacuum better than 10^{-2} mbar. A heat flux gauge was placed below the bottom sample as shown in Fig. 13 to have an assessment of the heat transfer rate through the sink.

The heat flow through the specimen was maintained at about 5 Watts for the experiments. The thermal path downward through the specimen had smaller thermal resistance compared to the thermal path upward through the pointed loading bolt. The heat transfer through the specimen was determined using the measured temperature and one-dimensional Fourier equation and compared with the power input to the heater. Values were about the same indicating that transverse and upward heat flow through the loading mechanism would be negligibly small. The radiation loss to the surrounding was minimized by covering the test pieces using a bright aluminium foil. The upper limit of the measured heat loss was within 12%.

The assumption of steady state was taken to correspond to a situation when maximum temperature change over a period of five minutes was less than 0.1 °C. In practice

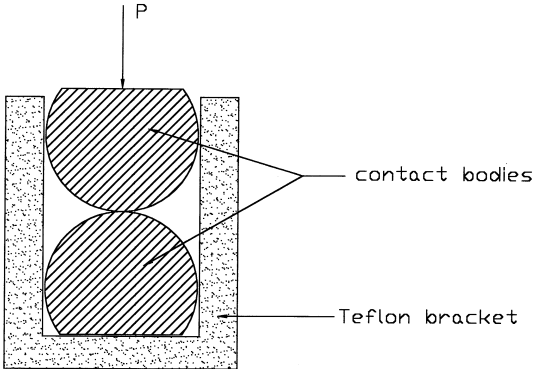

Fig. 12. Teflon fixture for sample holding

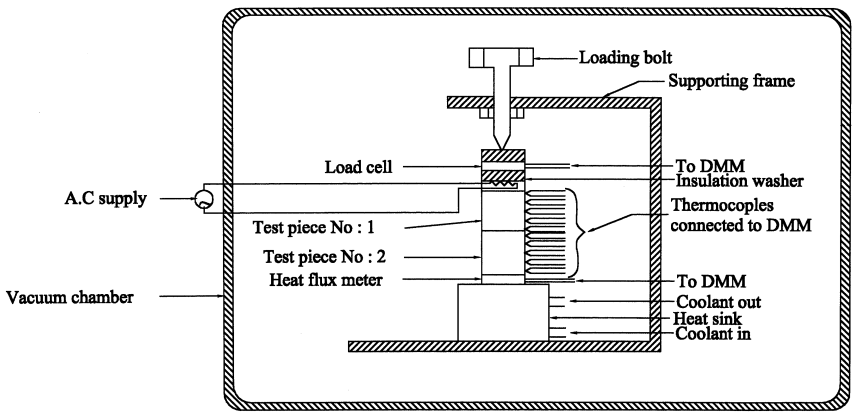

Fig. 13. Experimental set-up

steady state condition was reached within about four and a half hours. Lower contact area at the joint necessitated higher transient times.

8
Uncertainty in measurements

All the thermocouples were fabricated in the laboratory and were calibrated using highly accurate microprocessor controlled temperature bath prior to use. The interfacial temperature difference in the experiments varied between 7 °C and 29 °C and the mean interfacial temperature varied between 45 °C to 67 °C.

The uncertainties in measurements are the temperature differences, the error in locating the thermocouples and the magnitude of heat flow through the test specimen. The maximum uncertainty is associated with experiments having highest contact area across the joint. This condition result in the smallest temperature drop across the interface. The maximum uncertainty in the differential temperature is ±0.3 °C for the smallest temperature difference of 7 °C and corresponds to approximately 5% uncertainity. The heat evolution was taken to be known within 12% during tests. The largest uncertainty in measured thermal contact conductance was therefore $[0.05^2 + 0.12^2]^{0.5} = 13\%$.

9
Comparison of predictions with measured data

In all, fifteen set of data were prepared using the experimental set-up, five each for cylindrical aluminium and stainless steel joints and five for stainless steel spherical contact. The measured data are compared with the predicted values in Fig. 14. The uncertainty of the measured data is also indicated in the figure. The experimental measurement is seen to agree very closely with the prediction. The thermal contact conductance of aluminium contact is seen to be higher than that of the stainless steel joint and is to be anticipated in view of the higher deformed contact area. The predictions at no load conditions are almost the same as the experimentally measured value. At higher values of contact pressure there seems to be a slight under-prediction. This is in line with that observed for the case of flat surface joint [5] and calls for a re-look at the deformation model for contacting asperities and flow of metal at high contact pressures. The assumption of ideally shaped asperity contact (Fig. 2) could also lead to lower contact area resulting in reduced

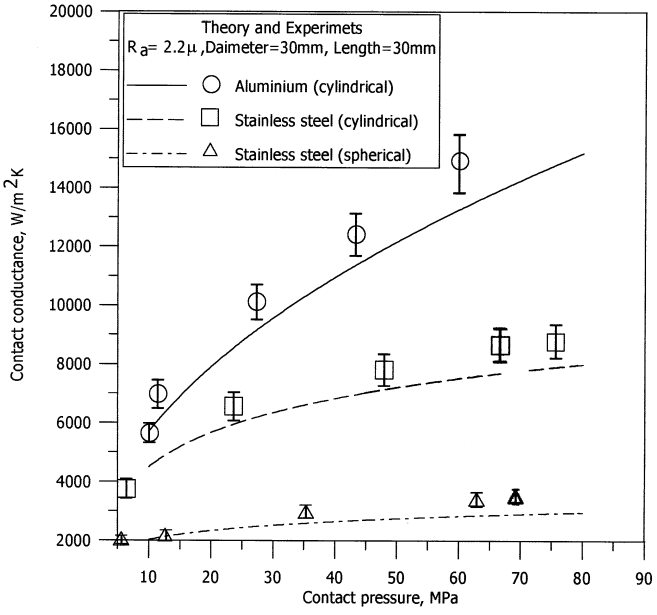

Fig. 14. Comparison of experimental results with predictions

conductance. However, the scatter in the measured data is in general within the measurement accuracy of the experiments.

10
Conclusion

A theoretical model based on randomly occurring contacts between asperities on surfaces of cylindrical and spherical bodies has been developed to predict the thermal contact conductance. The macro contact area corresponding to curvilinear surfaces in contact and the micro contact area for surface roughness is modeled. The Monte-Carlo simulation is used to approximate the possible area of contact between the contacting surfaces within the Hertzian elliptical contact region. The predicted results in the limit of infinite radius of curvature reproduce to the values obtained in earlier studies for flat surfaces in contact with each other. The predicted results of contact conductance for curvilinear surfaces were lower by almost an order of magnitude compared to those obtained for conforming flat surfaces. Among the curved surfaces in contact, the highest contact conductance was for cylinder

to flat surface contact while the lowest was for sphere to sphere contact.

The results obtained by the theoretical model is verified by generating experimental results for contact conductance with stainless steel and aluminium cylindrical contacts and a pair of stainless steel spherical contacts. Good agreement is observed between the experimentally measured conductance and theoretical predictions. At high loads the theory somewhat under-predicts the contact conductance suggesting that improved models for deformation of asperities at very high values of contact pressures may be necessary.

References

1. Clausing AM; Chao BT (1965) Thermal contact resistance in vacuum environment. ASME J Heat Transfer 87: 243–251
2. Mikic BB (1974) Thermal contact conductance; theoretical considerations. Int J Heat Mass Transfer 17: 205–214
3. Rostami AA; Hassan AY; Lim PC (2001) Parametric study of thermal constriction resistance. Heat Mass Transfer 37: 5–10
4. Leung M; Hsieh CK; Goswami DY (1998) Prediction of thermal contact conductance in vacuum by statistical mechanics. ASME J Heat Transfer 120: 51–57
5. Sunil Kumar S; Ramamurthi K (2001) Prediction of thermal contact conductance in vacuum using Monte-Carlo simulation. J Thermophys Heat Transfer 15: 27–33
6. Madhusudana CV (1999) Thermal contact conductance of cylindrical joints. Int J Heat Mass Transfer 42: 1273–1287
7. Sheffield TJ; Wood RA; Sauer HJ Jr (1989) Experimental investigation of thermal contact conductance of finned tube contacts. Exp Therm Fluid Sci 2: 107–121
8. Dart DM (1959) Effect of fin bond on heat transfer. ASHRAE J 1: 67–71
9. Gardner KA; Carnavos TC (1960) Thermal contact conductance in finned tubings. Trans ASME J Heat Transfer 82: 279–293
10. Kulkarni MV; Young EH (1966) Bimetallic finned tube. Chem Engg Prog 62(7): 68–71
11. Kitscha WW; Yovanovich MM (1975) Experimental investigation on the overall thermal resistance of sphere-flat contacts. Heat transfer with thermal control application. Progress Astronautics Aeronautics 39: 93–110
12. Fischer NJ; Yovanovich MM (1989) The constriction resistance of sphere/layered flat contacts: theory and experiments. J Heat Transfer 109: 249–256
13. Bejan A (1989) Theory of rolling contact heat transfer. J Heat Transfer 111: 257–262
14. Greenwood JA; Tripp JH (1967) The elastic contact of rough spheres. ASME J Appl Mech 34:153–159
15. Schneider GE; Strong AB; Yovanovich MM (1977) Transient thermal response of two bodies communicating through a small circular contact area. Int J Heat Mass Transfer 20: 301–307
16. Yovanovich MM; Kitscha WW (1974) Modeling the effect of air and oil upon the thermal resistance of a sphere-flat contact. Thermophysics and spacecraft thermal control. Prog Astronautics Aeronautics 35: 293–319
17. Seely FB; Smith JO (1963) Advances in mechanics of materials, Chapter 11, Wiley, NY
18. Timoshenko SP; Goodier JN (1970) Theory of elasticity, 3rd edn, McGraw-Hill, New York, pp 416
19. Konhauser M (1951) A note on elastic deformation. ASME J Appl Mech 18: 251–252
20. Yovanovich MM (1969) Overall constriction resistance between contacting, rough, wavy walls. Int J Heat Mass Transfer 12: 1517–1520
21. Thomas TR; Sayles RS (1975) Random process analysis of the effect of waviness on thermal contact resistance. Prog Astronautics Aeronautics 39: 3–20
22. Madhusudana CV (1996) Thermal contact conductance. Mechanical Engineering Series, Springer-Verlag, New York, pp 35
23. Marotta EE; Fletcher LS (2001) Thermal contact resistance models of non-flat, roughened surfaces with metallic coatings. ASME J Heat Transfer 123: 11–23
24. Sunil Kumar S; Ramamurthi K (2002) Control of thermal contact conductance by surface coatings. Proceedings of the 16th National and 5th ISHMT-ASME Heat and Mass Transfer Conference, pp 221–228, January, Calcutta